J. Fluid Mech. (1999), *vol.* 395, *pp.* 161–180. Printed in the United Kingdom

The concept of block-effective macrodispersivity and a unified approach for grid-scale- and plume-scale-dependent transport

By Y. RUBIN[1], A. SUN[1], R. MAXWELL[1,2] AND A. BELLIN[3]

[1] Department of Civil and Environmental Engineering, University of California, Berkeley, CA 94720, USA

[2] Lawrence Livermore National Laboratory, CA 94550, USA

[3] Department of Civil and Environmental Engineering, University of Trento, Via Belenzani 12, 38100 Trento, Italy

(Received 8 August 1998 and in revised form 30 March 1999)

We present a new approach for modelling macrodispersivity in spatially variable velocity fields, such as exist in geologically heterogeneous formations. Considering a spectral representation of the velocity, it is recognized that numerical models usually capture low-wavenumber effects, while the large-wavenumber effects, associated with subgrid block variability, are suppressed. While this suppression is avoidable if the heterogeneity is captured at minute detail, that goal is impossible to achieve in all but the most trivial cases. Representing the effects of the suppressed variability in the models is made possible using the proposed concept of block-effective macrodispersivity. A tensor is developed, which we refer to as the block-effective macrodispersivity tensor, whose terms are functions of the characteristic length scales of heterogeneity, as well as the length scales of the model's homogenized areas, or numerical grid blocks. Closed-form expressions are developed for small variability in the log-conductivity and unidirectional mean flow, and are tested numerically. The use of the block-effective macrodispersivities allows conditioning of the velocity field on the measurements on the one hand, while accounting for the effects of unmodelled heterogeneity on the other, in a numerically reasonable set-up. It is shown that the effects of the grid scale are similar to those of the plume scale in terms of filtering out the effects of portions of the velocity spectrum. Hence it is easy to expand the concept of the block-effective dispersivity to account for the scale of the solute body and the pore-scale dispersion.

1. Introduction

Macrodispersion tensors are commonly used for modelling dispersion of solute bodies in spatially variable velocity fields. The theory of macrodispersivity has been explored in by Dagan (1989), Gelhar (1993) and Rubin (1990, 1997). A fundamental assumption associated with this concept is that the velocity fields are represented only through their expected value, and that the macrodispersivity tensor accounts for all the effects of unmodelled spatial variability of the velocity field on mixing. In many real-life applications, measurements of the conductivity or the velocity are available, and it is only reasonable to incorporate them into the model, especially due to the great expense involved. Conditioning models on measured data, however, violates the

requirement that the velocity field is modelled through its expected value: the inclusion of measurements leads to local deviation of the velocity field from its expected value. The risk is that the effects of spatial variability will be duplicated, and will appear as dispersive fluxes and as advective fluxes. An alternative, consistent approach, which we pursue here, is to condition the models on the available measurements, and to remove the effects which are modelled implicitly from the macrodispersion coefficients.

Stochastic modelling often calls for Monte Carlo simulation, requiring repeated generation of the conductivity field, followed by numerical solutions of the flow and transport problems. To capture accurately the effects of spatial variability, a very fine grid is required, with typical grid block scale being equal to only a small fraction of the log-conductivity integral scale. The ensuing computational burden may be overwhelming sometimes, and the tendency is to reduce the effort by increasing the grid block scale. The loss of resolution results in homogenization of relatively large areas, and in elimination of the subgrid-scale variability from consideration. Hence measures should be taken to account for the effects which are eliminated by homogenization. Here we can also envision a modelling approach whereby the effects of spatial variability are captured in part by modelling directly the heterogeneity of the conductivity field, and the rest through dispersive fluxes.

Hence, whether we are interested in conditioning of models on measurements, or in reducing grid block resolution, the ability to separate the effects of modelled and unmodelled variability is important, and is the main focus of this study.

2. Mathematical statement of the problem

In this study we consider flow and transport in saturated heterogeneous media. The general approach for treating the effects of media's heterogeneity and prediction uncertainty (Dagan 1989) is to model the hydrogeological variables as space random functions (SRFs), defined through their statistical moments.

Consider a variable such as the log-conductivity $Y(\boldsymbol{x})$, where $\boldsymbol{x}$ denotes the spatial coordinate. In this paper, boldface letters denote vectors and capital letters denote SRFs. Y is defined through its expected value $m_Y = \langle Y \rangle$, where angled brackets denote the expected value operator, and its two-point spatial covariance $C_Y(\boldsymbol{x}, \boldsymbol{x}')$:

$$C_Y(\boldsymbol{x}, \boldsymbol{x}') = \langle Y'(\boldsymbol{x}) Y'(\boldsymbol{x}') \rangle, \tag{1}$$

where $Y' = Y - m_Y$ is the local fluctuation of Y from its expected value. In the case of stationary variability, $C_Y(\boldsymbol{x}, \boldsymbol{x}') = C_Y(|\boldsymbol{r}|)$ where $\boldsymbol{r} = \boldsymbol{x} - \boldsymbol{x}'$ is the lag distance. The spatial variability of Y can also be described in the wavenumber domain, through its spectrum $S_Y(\boldsymbol{k})$, which is the Fourier transform of $C_Y(\boldsymbol{r})$, where k_i is the wavenumber corresponding to r_i.

The spatial covariance C_Y yields two important measures of the variability of Y. The first is the variance of Y, σ_Y^2, which is obtained by substituting $\boldsymbol{x} = \boldsymbol{x}'$ in $C_Y(\boldsymbol{x}, \boldsymbol{x}')$. Additionally, a measure of the directional spatial persistence of Y is provided in the form of the integral scale $I_{Y,i}$, which is defined as follows:

$$I_{Y,i} = \int_0^\infty C_Y(r_i)\, \mathrm{d}r_i, \tag{2}$$

where r_i is the modulus $|x_i - x_i'|$, with the subscript i denoting a Cartesian direction, $i = 1, \ldots, m$, with m being the space dimensionality. Most geological formations are characterized by different integral scales in different directions (Rubin *et al.* 1998).

The identification of C_Y requires a large number of measurements. Since C_Y is

a functional which is defined for various r_i, its accurate identification requires that the samples are taken over large areas, and in a way which captures the covariance for different r_i and for all i. Once a model of spatial variability is defined, it can be used for modelling the effects of the spatial variability on processes such as flow and contaminant transport. A common approach is Monte Carlo numerical simulations. In a Monte Carlo study, an image of the hydraulic conductivity is generated, subject to the target statistics such as m_Y and C_Y. That usually implies generating Y-values at nodes which are a distance λ_i apart. The image is then used as an input to flow and transport simulators, and a value of the desired parameter, such as the concentration of a certain contaminant at some location. This process is repeated numerous times, until a histogram of the desired variable is obtained.

To reproduce correctly the effects of the spatial variability, a detailed, high-resolution image of the aquifer needs to be generated. Previous studies (Ababou *et al.* 1989; Bellin, Salandin & Rinaldo 1992; Chin 1997) indicates that in the case of very large plumes, spatial resolution λ_i of the order $0.25I_{Y,i}$ is sufficient, implying that the displacement of the solute body and its dispersion are quite insensitive to spatial variability at a smaller scale. When dealing with smaller solute bodies, obviously this is no longer the case, and an even finer resolution may be needed (Dykkar & Kitanidis 1992).

Generating or sampling Y-values at discrete nodes limits the ability to either reproduce or capture the desired spatial statistics. Consider the case of Y which is defined by the spectrum $S_Y(\boldsymbol{k})$. According to the Nyquist sampling theorem (Bras & Rodriguez-Iturbe 1985; Beckie, Aldama & Wood 1996), the spacing between Y-values, which constitutes the sampling frequency, defines an upper cut-off value for the frequencies which are recognized. Sampling the Y-field with spacing λ_i will not reproduce accurately the spectrum corresponding to frequencies higher than $(2\lambda_i)^{-1}$. If we represent the effect of this cut-off as a sharp low-pass filter, the spectrum reproduced by generating Y-values over nodes with spacing λ_i is (Beckie *et al.* 1996):

$$S_N(\boldsymbol{k}) = \begin{cases} S_Y(\boldsymbol{k}) & \text{for } k_i \leqslant \dfrac{\pi}{\lambda_i}, \quad i = 1, \ldots, m \\ 0 & \text{otherwise.} \end{cases} \tag{3}$$

The definitions of the Fourier transform pair employed here as well as of the relationship between spectra and *radial* spectra are given in the Appendix. The wavenumber π/λ_i corresponds to the highest observable frequency $f_i = (2\lambda_i)^{-1}$ (Bras & Rodriguez-Iturbe 1985). The low-pass filter (3) is only an approximate representation of the effects of discretization, since the small-scale fluctuations are aliased into the sampled frequencies. A graphical representation of the invisible and visible spectrum is given on figure 1.

As the spacing λ_i decreases, the simulated spectrum S_N approaches the target spectrum S_Y. However, simulation with small λ_i implies a very fine grid and a large computational effort. On the other hand, simulating flow and transport over a field characterized by a spectrum S_N which departs largely from the target spectrum S_Y will lead to large errors and discrepancies between the simulated and actual values of the parameters of interest such as the concentration, due to the elimination of the large-wavenumber features.

So far we have considered λ_i to be the spacing between generated Y-values in a Monte Carlo simulation. The scale λ_i can also represent the average spacing of the measurements taken in the field. Due to the large expenditure associated with procurement of the measurements, the modeller is motivated to condition the model

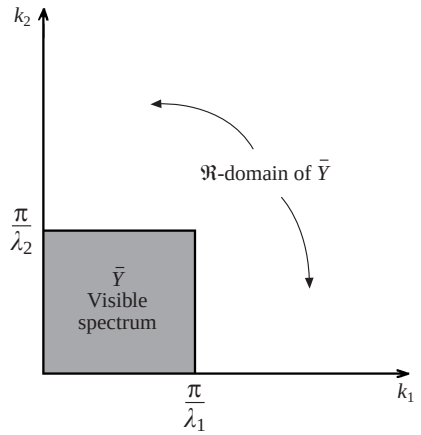

FIGURE 1. Illustration of the sharp, low-pass filter in two-dimensional space. $\widetilde{Y}$ denote the variability which is wiped out due to partial sampling of block homogenization. $\overline{Y}$ denotes the complementary variability.

on the measurements while accounting for the unsampled variability. Hence, whether we are dealing with a λ_i value which represents numerical constraints or a field situation, in both cases the lost portion of the spectrum is of a great concern.

That dichotomy between the need for high resolution and its implications in terms of costs can be potentially reconciled if steps are taken to account for the 'lost' variability. The goal of this paper is to investigate this option and to incorporate the effects of the unmodelled spectrum on transport without resorting to fine-scale grid discretization, using the concept of block dispersivities.

The basic idea is to represent Y as follows:

$$Y(\boldsymbol{x}) = m_Y + \overline{Y}(\boldsymbol{x}) + \widetilde{Y}(\boldsymbol{x}), \tag{4}$$

where $\overline{Y}$ is a zero-mean fluctuation, characterized by the spectrum $S_{\overline{Y}}$, representing the variability modelled/captured by simulations and or measurements, and $\widetilde{Y}$ is the zero-mean fluctuation characterized by the spectrum $S_{\widetilde{Y}}$, which represents the subgrid variability. From the previous discussion, $S_{\overline{Y}}$ is analogous to S_N, while $S_{\widetilde{Y}}$ represents the complementary, invisible spectrum shown on figure 1. To grasp the effect of the invisible spectrum $S_{\widetilde{Y}}$ on transport, its effect on variables such as hydraulic head and velocity needs to be investigated, see § 3.

Note that since the sum of $\overline{Y}$ and $\widetilde{Y}$ equals $Y - m_Y$, we have that

$$\sigma_Y^2 = \langle(\overline{Y} + \widetilde{Y})^2\rangle; \tag{5}$$

however, no order relationship exists between $\overline{Y}$ and $\widetilde{Y}$, and each of these variables is of the order of the standard deviation σ_Y. They are characterized by different integral scales: $\overline{Y}$ represents the low-frequency variability, and its integral scale is much larger than that of $\widetilde{Y}$. In the subsequent derivation, we omit the reference to the space coordinates unless deemed necessary.

3. The significance of subgrid variability

We start by considering the effects of $\overline{Y}$ and $\widetilde{Y}$ on the hydraulic head H. In doing that, we follow and extend the ideas of Dagan (1984) and Ababou & Gelhar (1990).

Assuming steady-state divergence-free flow, the relationship between the head and log-conductivity is given by (Dagan 1984):

$$\nabla^2 H + \nabla H \cdot \nabla Y = 0. \tag{6}$$

To identify the hydraulic head responses which correspond to $\overline{Y}$ and $\widetilde{Y}$, we define the hydraulic head through the truncated series

$$H(\boldsymbol{x}) = \left\langle H(\boldsymbol{x}; \sigma_Y^0) \right\rangle + \overline{h}(\boldsymbol{x}; \sigma_Y^1) + \tilde{h}(\boldsymbol{x}; \sigma_Y^1) + O(\sigma_Y^2) \tag{7}$$

and attempt to define the effects of $\overline{Y}$ and $\widetilde{Y}$ on $\overline{h}$ and $\tilde{h}$. Assuming that m_Y is stationary, and substituting (4) and (7) in (6) leads to

$$\nabla^2 \langle H \rangle + \nabla^2 \overline{h} + \nabla^2 \tilde{h} + (\nabla \langle H \rangle + \nabla \overline{h} + \nabla \tilde{h}) \cdot \nabla (\overline{Y} + \widetilde{Y}) = 0. \tag{8}$$

Equation (8) is a stochastic partial differential equation, since all variables in (8), with the exception of $\langle H \rangle$, are random functions. We can focus on the relationship between the small-scale $\tilde{h}$ and $\widetilde{Y}$ by conditional averaging of (8) on the large-scale variables $\overline{h}$ and $\overline{Y}$. The resulting conditional mean equation

$$\nabla^2 \langle H \rangle + \nabla^2 \overline{h} + \nabla \langle H \rangle \cdot \nabla \overline{Y} + \nabla \overline{h} \cdot \nabla \overline{Y} = -\langle \nabla \tilde{h} \cdot \nabla \widetilde{Y} \rangle \tag{9}$$

can then be subtracted from (8), leading to an equation relating $\tilde{h}$ and $\widetilde{Y}$, conditional on the large-scale fluctuations in both head and log-conductivity:

$$\nabla^2 \tilde{h} + \nabla \langle H \rangle \cdot \nabla \widetilde{Y} + \nabla \overline{h} \cdot \nabla \widetilde{Y} + \nabla \tilde{h} \cdot \nabla \overline{Y} = -(\nabla \tilde{h} \cdot \nabla \widetilde{Y} - \langle \nabla \tilde{h} \cdot \nabla \widetilde{Y} \rangle). \tag{10}$$

This equation can be simplified by neglecting products of random fluctuations, yielding

$$\nabla^2 \tilde{h} + \nabla \langle H \rangle \cdot \nabla \widetilde{Y} + \nabla \overline{h} \cdot \nabla \widetilde{Y} + \nabla \tilde{h} \cdot \nabla \overline{Y} \approx 0. \tag{11}$$

At the next step we seek a solution for $\overline{h}$ in terms of $\overline{Y}$ and $\langle H \rangle$. The order relationship defined in (7) suggests

$$\nabla^2 \langle H \rangle = 0, \tag{12}$$

which we substitute in (9), and by discarding products of fluctuations, we obtain

$$\nabla^2 \overline{h} = \boldsymbol{J} \cdot \nabla \overline{Y} \tag{13}$$

where $\boldsymbol{J} = -\nabla \langle H \rangle$. Integrating (13) once leads to

$$\nabla \overline{h} = \boldsymbol{J} \Gamma(\overline{Y}), \tag{14}$$

where Γ is an operator (see Dagan 1985, equation 3g), and $\Gamma(\overline{Y})$ is of order σ_Y. Equation (14) can now be coupled with (11) to yield

$$\nabla^2 \tilde{h} - \boldsymbol{J} \cdot \nabla \widetilde{Y} + (\boldsymbol{J} \Gamma(\overline{Y})) \cdot \nabla \widetilde{Y} + \nabla \tilde{h} \cdot \nabla \overline{Y} = 0. \tag{15}$$

For convenience, we transform (15) into Fourier space, and using the vector $\boldsymbol{k}$ to denote the wavenumber vector, we obtain

$$\tilde{h}(\boldsymbol{k}) = \frac{\boldsymbol{J}(1 - \Gamma(\overline{Y})) \cdot \mathrm{i}\boldsymbol{k} \widetilde{Y}(\boldsymbol{k})}{k^2 + \mathrm{i}\boldsymbol{k} \cdot \nabla \overline{Y}} \tag{16}$$

where $k^2 = k_j k_j$, $j = 1, \ldots, m$. In (16), the summation convention applies, and i is the imaginary unit. Equation (16) contains products of perturbations, which we shall carry forward until further simplification. Equation (16) is a slight variation on a result obtained by Ababou & Gelhar (1990).

Recalling that $\tilde{h}$ represents the variability lost due to discretization, we learn from (16) that the least effect on accurate reproduction of the head surface will occur in regions of relatively high $\overline{Y}$, especially near $\overline{Y} \approx 1$, which are regions of relatively persistent high conductivity, where the high-frequency head response vanishes. The largest loss in variability will occur at the low-conductivity areas, where $\overline{Y}$ is negative. The local gradient of $\overline{Y}$ also plays an important role, since larger gradients of $\overline{Y}$ reduce $\tilde{h}$.

At the next step we proceed to develop the local velocity response to large- and small-scale fluctuations in the log-conductivity. Starting with Darcy's law:

$$\boldsymbol{V} = -\frac{1}{n} K \nabla H, \tag{17}$$

and combining (17) with (4) and (7), we obtain at order σ_Y

$$\boldsymbol{V} = \frac{K_G}{n}(1 + \boldsymbol{J}\overline{Y} + \boldsymbol{J}\widetilde{Y} - \nabla\overline{h} - \nabla\tilde{h}) \tag{18}$$

after elimination of products of perturbations. $K_G = \exp(m_Y)$ is the geometric mean of the conductivity, and n is the porosity. The last equation allows the velocity response to the large-scale log-conductivity fluctuation

$$\bar{\boldsymbol{u}} = \frac{K_G}{n}(\boldsymbol{J}\overline{Y} - \nabla\overline{h}) \tag{19}$$

and to the small-scale log-conductivity fluctuation

$$\tilde{\boldsymbol{u}} = \frac{K_G}{n}(\boldsymbol{J}\widetilde{Y} - \nabla\tilde{h}) \tag{20}$$

to be defined. Using tensorial notation and moving to Fourier space, the local velocity fluctuation becomes

$$\tilde{u}_j(\boldsymbol{k}) = \frac{K_G}{n}[J_j \widetilde{Y}(\boldsymbol{k}) + \mathrm{i}k_j \tilde{h}(\boldsymbol{k})]. \tag{21}$$

Using (16), an explicit expression for $\tilde{u}_j$ in terms of the small- and large-scale fluctuations of the log-conductivity is obtained:

$$\tilde{u}_j(\boldsymbol{k}) = \frac{K_G}{n}\left\{J_j + \mathrm{i}k_j\left[\frac{J_q(1 - \Gamma(\overline{Y}))\mathrm{i}k_q}{k^2 + \mathrm{i}\boldsymbol{k}\cdot\nabla\overline{Y}}\right]\right\}\widetilde{Y}(\boldsymbol{k}). \tag{22}$$

Note that the accurate interpretation of $\tilde{u}_j$ is that it is the small-scale (high-frequency) component of the velocity fluctuation, as a function of the small-scale component of the log-conductivity fluctuation, *conditional* to the large-scale (low-frequency) components of the log-conductivity fluctuations. All fluctuations are measured with respect to the relevant expected value. The conditioning renders $\tilde{u}_j$ non-stationary, since $\overline{Y}$ varies in space, and in fact $\tilde{u}_j(\boldsymbol{k}) = \tilde{u}_j(\boldsymbol{k}, \boldsymbol{x})$. Taking $\overline{Y} = 0$ in (22) and ignoring the tilde sign simplifies (22) and leads to the well-known expression by Dagan (1989), for velocity fluctuations in spatially variable, stationary aquifers.

Combining (22) with the identity given in the Appendix, the conditional radial spectrum of the small-scale velocity fluctuations is defined as follows:

$$\tilde{u}_{jl}(\boldsymbol{k}|\bar{\boldsymbol{u}}) = U_q U_p \left\{\delta_{jq} - \frac{k_j k_q}{k^2}\right\}\left\{\delta_{lp} - \frac{k_l k_p}{k^2}\right\} C_{\widetilde{Y}}(\boldsymbol{k}) \tag{23}$$

in terms of $C_{\overline{Y}}$, the radial spectrum of the wiped-out small-scale fluctuations. $\boldsymbol{U} = U_i$, $i = 1, \ldots, m$, is the mean velocity vector. This expression is similar to the one defined previously by Dagan (1989), except that it pertains to the small-scale velocity variations. Again referring to Appendix A, (23) is the Fourier transform of the *Eulerian* velocity covariance $\tilde{u}_{jl}(\boldsymbol{x}, \boldsymbol{x}'|\bar{\boldsymbol{u}})$. In developing (23), terms of order $(\sigma_Y)^n$, with $n > 2$ were removed for consistency. The most consequential aspect of the higher-order terms removal is the elimination of non-stationarity. This mathematical form is identical to the spectrum of the actual velocity field (Dagan 1989; Gelhar 1993), the only difference being the replacement of the complete spectrum with the truncated one.

As an example, consider the spectrum of the velocity components orthogonal to the mean flow direction, which we take along the x_1-axis:

$$\tilde{u}_{22}(\boldsymbol{k}, \boldsymbol{x}|\bar{\boldsymbol{u}}) = U_1^2 \left\{ \frac{k_1 k_2}{k^2} \right\}^2 C_{\tilde{Y}}(\boldsymbol{k}). \tag{24}$$

We can conclude now that as long as a non-zero $S_{\tilde{Y}}$ exists, the numerically simulated lateral variability spectrum of the velocity will underestimate the actual one.

4. The effects of subgrid variability on macrodispersion

To capture the effects of the subgrid variability on transport, we consider its effects on macrodispersion. The objective is to model the macrodispersive flux which is lost due to the modelled small-scale variability in the velocity field.

Consider the displacement of a solute particle. Its total displacement follows the Lagrangian description

$$X_j(t) = \int_0^t V_j(t')\,\mathrm{d}t', \quad j = 1, \ldots, m. \tag{25}$$

Taking expected value of (25) and subtracting from (25), with the aid of (18), (19) and (20), the difference between the displacement and its expected value is obtained:

$$X'_j(t) = \int_0^t \bar{u}_j(t')\,\mathrm{d}t' + \int_0^t \tilde{u}_j(t')\,\mathrm{d}t', \quad j = 1, \ldots, m, \tag{26}$$

expressed as the sum of the high- and low-frequency components of the velocity fluctuation. Since both $\tilde{\boldsymbol{u}}$ and $\bar{\boldsymbol{u}}$ are of order σ_Y, then so is $\boldsymbol{X}'$.

To capture the effects of the small-scale variability, we shall consider the behaviour of the $\tilde{\boldsymbol{u}}$-field conditional to a given $\bar{\boldsymbol{u}}$-field. Under this definition, the only random component of the displacement is the second term on the right-hand side of (26), and the corresponding random component of the displacement is

$$\widetilde{X}'_j(t|\bar{\boldsymbol{u}}) = \int_0^t \tilde{u}_j(t'|\bar{\boldsymbol{u}})\,\mathrm{d}t', \quad j = 1, \ldots, m. \tag{27}$$

Due to its randomness, this quantity can only be defined through its moments. From the properties of $\tilde{\boldsymbol{u}}$ we can establish that $\langle \widetilde{X}'_j(t|\bar{\boldsymbol{u}}) \rangle = 0$. The conditional displacement variance is available from squaring (27) and taking expected value, leading to the displacement variance:

$$\begin{aligned} \widetilde{X}_{ij}(t|\bar{\boldsymbol{u}}) = \langle \widetilde{X}'_i(t|\bar{\boldsymbol{u}}) \widetilde{X}'_j(t|\bar{\boldsymbol{u}}) \rangle &= \int_0^t \int_0^t \langle \tilde{u}_i(t'|\bar{\boldsymbol{u}}) \tilde{u}_j(t'|\bar{\boldsymbol{u}}) \rangle \,\mathrm{d}t'\,\mathrm{d}t'' \\ &= \int_0^t \int_0^t \tilde{v}_{ij}(t', t''|\bar{\boldsymbol{u}})\,\mathrm{d}t'\,\mathrm{d}t'', \end{aligned} \tag{28}$$

where $\tilde{v}_{ij}$ is the Lagrangian velocity covariance of the small-scale fluctuations $\tilde{\boldsymbol{u}}$. A fundamental difficulty that we face here resides in the fact that Lagrangian velocity covariances are generally not available in subsurface applications. However, since

$$\tilde{v}_{ij}(t,t'|\bar{\boldsymbol{u}}) = \tilde{v}_{ij}[\boldsymbol{X}(t),\boldsymbol{X}(t')|\bar{\boldsymbol{u}}] = \tilde{v}_{ij}[\langle \boldsymbol{X}(t)\rangle + \boldsymbol{X}'(t), \langle \boldsymbol{X}(t')\rangle + \boldsymbol{X}'(t')|\bar{\boldsymbol{u}}] \tag{29}$$

we get the following relationship between the Lagrangian and Eulerian covariances (Dagan 1989):

$$\tilde{v}_{ij}(t,t'|\bar{\boldsymbol{u}}) = \tilde{u}_{ij}[\langle \boldsymbol{X}(t)\rangle, \langle \boldsymbol{X}(t')\rangle|\bar{\boldsymbol{u}}] + O(\sigma_Y^3) \tag{30}$$

which allows the statement

$$\widetilde{X}_{ij}(t|\bar{\boldsymbol{u}}) = \int_0^t \int_0^t \tilde{u}_{ij}[\langle \boldsymbol{X}(t')\rangle, \langle \boldsymbol{X}(t'')\rangle|\bar{\boldsymbol{u}}]\,\mathrm{d}t'\,\mathrm{d}t''. \tag{31}$$

The significant advantage of (31) over (28) is the removal of nonlinearity. It is recalled that $\tilde{u}_{ij}(\boldsymbol{x},\boldsymbol{x}'|\bar{\boldsymbol{u}})$ is the inverse Fourier transform of $\tilde{u}_{ij}(\boldsymbol{k}|\bar{\boldsymbol{u}})$, defined previously in (23). Due to the stationarity of $\tilde{u}_{ij}(\boldsymbol{x},\boldsymbol{x}'|\bar{\boldsymbol{u}})$, see (23), and limiting our attention to uniform-in-the-mean flow fields, we can modify (31) to the form

$$\widetilde{X}_{ij}(t'|\bar{\boldsymbol{u}}) = \int_0^t \int_0^t \tilde{u}_{ij}[\langle \boldsymbol{X}(t')\rangle - \langle \boldsymbol{X}(t'')\rangle|\bar{\boldsymbol{u}}]\,\mathrm{d}t'\,\mathrm{d}t'' = \int_0^t \int_0^t \tilde{u}_{ij}[U(t'-t'')]\,\mathrm{d}t'\,\mathrm{d}t'' \tag{32}$$

which no longer requires any conditioning.

For Gaussian displacements $\widetilde{\boldsymbol{X}}$, it has been shown by Dagan (1989) that a macrodispersion coefficient can be defined as follows:

$$\widetilde{D}_{ij}(t) = \frac{\mathrm{d}\widetilde{X}_{ij}}{2\,\mathrm{d}t}, \quad i,j = 1,\ldots,m. \tag{33}$$

Considering (18), and if Y is Gaussian, the velocity, and hence the displacement, are Gaussian at any travel time. For a non-Gaussian field, the displacement becomes Gaussian by merit of the central limit theorem after a certain travel time. $\widetilde{D}_{ij}$ in (33) can be used to account for the consequences of the wiped-out spectrum, or the subgrid-scale variability, and hence we refer to it as the 'block-effective macrodispersion tensor'. The qualifier 'block effective' serves to distinguish it from the macrodispersion coefficients (Dagan 1989; Gelhar 1993). The relationship between the two will be discussed at the end of this section.

A fundamental issue we address next concerns the conditions under which (33) holds, or in other words, the conditions under which the single particle displacement statistics can be used for computing macrodispersion coefficients. This issue has been investigated in the study by Dagan (1991), concluding that for (33) to qualify, the plume must be ergodic, implying a width of several integral scales in the direction normal to mean flow. These conditions are quite restrictive, in general. However, the integral scale of $\widetilde{Y}$, $I_{\widetilde{Y}}$, is smaller than I_Y, the integral scale of Y, and hence ergodicity with regard to the wiped-out variability is attained under less restrictive conditions: plumes that are non-ergodic with respect to I_Y can be ergodic with respect to $I_{\widetilde{Y}}$. This idea is demonstrated in figure 2. This figure shows the ratio $I_{\widetilde{Y}}/I_Y$ as a function of the ratio λ/I_Y. $I_{\widetilde{Y}}$ increases with λ and approaches I_Y for large λ, as the wiped-out spectrum approaches the total spectrum of the variability in the aquifer.

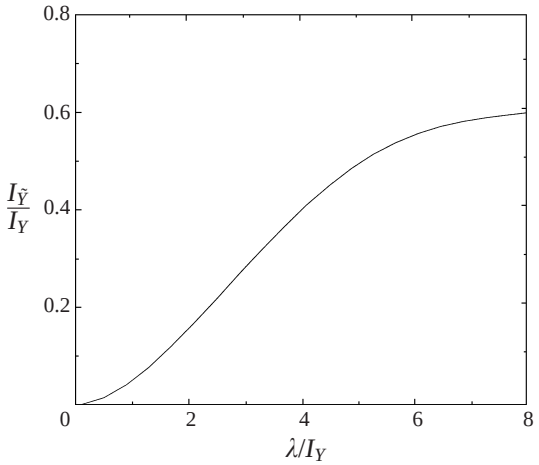

FIGURE 2. The ratio between the integral scale of $\widetilde{Y}$ and that of Y as a function of the block scale.

Since

$$\widetilde{D}_{ij}(t) = \int_0^t \tilde{u}_{ij}(t')\,\mathrm{d}t' \tag{34}$$

we can combine (27) and (3) with (35) to get the general expression for the block-effective macrodispersion coefficient:

$$\widetilde{D}_{ij}(t) = \frac{1}{(2\pi)^{m/2}} \int_0^t \int_{\mathfrak{R}} \cdots \int \mathrm{e}^{-\mathrm{i}\boldsymbol{k}\cdot\boldsymbol{U}t} \tilde{u}_{ij}(\boldsymbol{k})\,\mathrm{d}\boldsymbol{k}\,\mathrm{d}t \tag{35}$$

where $\mathfrak{R}$ is the domain of the wiped-out spectrum (see figure 1). A more explicit form is obtained by introducing (23), as follows:

$$\widetilde{D}_{ij}(t) = \frac{1}{(2\pi)^{m/2}} \int_0^t \left[\begin{array}{l} \displaystyle\int_{-\infty}^{\infty} \cdots \int_{-\infty}^{\infty} \mathrm{e}^{-\mathrm{i}\boldsymbol{k}\cdot\boldsymbol{U}t'} U_q U_p \left\{ \delta_{jq} - \frac{k_j k_q}{k^2} \right\} \\ \quad \times \left\{ \delta_{lp} - \frac{k_l k_p}{k^2} \right\} C_Y(\boldsymbol{k})\,\mathrm{d}\boldsymbol{k} \\ \displaystyle - \int_{-\pi/\lambda_1}^{\pi/\lambda_1} \cdots \int_{-\pi/\lambda_m}^{\pi/\lambda_m} \mathrm{e}^{-\mathrm{i}\boldsymbol{k}\cdot\boldsymbol{U}t'} U_q U_p \left\{ \delta_{jq} - \frac{k_j k_q}{k^2} \right\} \\ \quad \times \left\{ \delta_{lp} - \frac{k_l k_p}{k^2} \right\} C_Y(\boldsymbol{k})\,\mathrm{d}\boldsymbol{k} \end{array} \right] \mathrm{d}t' \tag{36}$$

and in a more compact form:

$$\widetilde{D}_{ij}(t) = \frac{1}{(2\pi)^{m/2}} \int_0^t \left[\int_{-\infty}^{\infty} \cdots \int_{-\infty}^{\infty} \mathrm{e}^{-\mathrm{i}\boldsymbol{k}\cdot\boldsymbol{U}t'} U_q U_p \left\{ \delta_{jq} - \frac{k_j k_q}{k^2} \right\} \times \left\{ \delta_{lp} - \frac{k_l k_p}{k^2} \right\} F(\boldsymbol{k}) C_Y(\boldsymbol{k})\,\mathrm{d}\boldsymbol{k} \right] \mathrm{d}t', \tag{37}$$

with

$$F(\boldsymbol{k}) = \begin{cases} 0, & |k_i| \leqslant \pi/\lambda_i \text{ for all } i \\ 1 & \text{otherwise} \end{cases}$$

acting as a filter function.

The first m-integral on the right-hand side of (36) is the well-known expression for the macrodispersion coefficient for ergodic plumes, documented in Gelhar & Axness (1983) and Dagan (1984), which we denote here as $D^*_{ij}(t)$. Thus we can simplify (36) to the following form:

$$\widetilde{D}_{ij}(t) = D^*_{ij}(t) - \frac{1}{(2\pi)^{m/2}} \int_0^t \left[\int_{-\pi/\lambda_1}^{\pi/\lambda_1} \cdots \int_{-\pi/\lambda_m}^{\pi/\lambda_m} \mathrm{e}^{-\mathrm{i}\boldsymbol{k}\cdot\boldsymbol{U}t'} U_q U_p \times \left\{ \delta_{jq} - \frac{k_j k_q}{k^2} \right\} \left\{ \delta_{lp} - \frac{k_l k_p}{k^2} \right\} C_Y(\boldsymbol{k})\, \mathrm{d}\boldsymbol{k} \right] \mathrm{d}t'. \tag{38}$$

Two limits of (38) are immediate. For $\lambda_i \to 0$, implying a very fine grid discretization, $\widetilde{D}_{ij} \to 0$, since all the effects of the spatial variability are modelled directly on the grid. For very large λ_i, $\widetilde{D}_{ij} \to D^*_{ij}$, since none of the heterogeneity is modelled directly, and it all needs to be modelled through macrodispersion coefficients.

In both cases, the macrodispersion coefficients are time dependent, and hence non-local. The non-locality is not an outcome of the invisible spectrum, and is rather general in the case of heterogeneous media. This definition of non-locality, reflecting the Lagrangian nature of our approach, is somewhat different from the one endorsed by Cushman and co-workers (Cushman, Deng & Hu 1995) and Neuman and co-workers (Neuman & Orr 1993). In their Eulerian approach, a constitutive theory '... is said to be non-local if it involves integrals over space and or time or derivatives of order higher than the first' (Hu, Deng & Cushman 1997).

5. Analytical results for planar flow

We consider the case of planar flow in a domain defined by an anisotropic, stationary exponential log-conductivity covariance C_Y:

$$C_Y(\boldsymbol{r}) = \sigma_Y^2 \exp\left[-\left(\frac{r_1^2}{I_1^2} + \frac{r_2^2}{I_2^2} \right)^{1/2} \right], \tag{39}$$

with I_1 and I_2 being the integral scales of the log-conductivity in the x_1- and x_2-directions, respectively. The mean flow direction is taken along the x_1-axis, and hence $\boldsymbol{U} = (U_1, 0)$. The corresponding radial spectrum is given by (Dagan 1989)

$$C_Y(\boldsymbol{k}) = \frac{\sigma_Y^2 I_1 I_2}{[1 + (I_1 k_1)^2 + (I_2 k_2)^2]^{3/2}}. \tag{40}$$

When combining (40) with (23) and (38) for $i = j = 1$, the longitudinal macrodispersion coefficient is obtained:

$$\widetilde{D}_{11}(t) = D^*_{11}(t) - \frac{2\sigma_Y^2 I_1 I_2 U_1^2}{\pi} \int_0^t \int_0^{\pi/\lambda_1} \int_0^{\pi/\lambda_2} \left(1 - \frac{k_1^2}{k^2} \right)^2 \times \frac{\cos(U_1 k_1 t')}{[1 + (I_1 k_1)^2 + (I_2 k_2)^2]^{3/2}}\, \mathrm{d}k_1\, \mathrm{d}k_2\, \mathrm{d}t'. \tag{41}$$

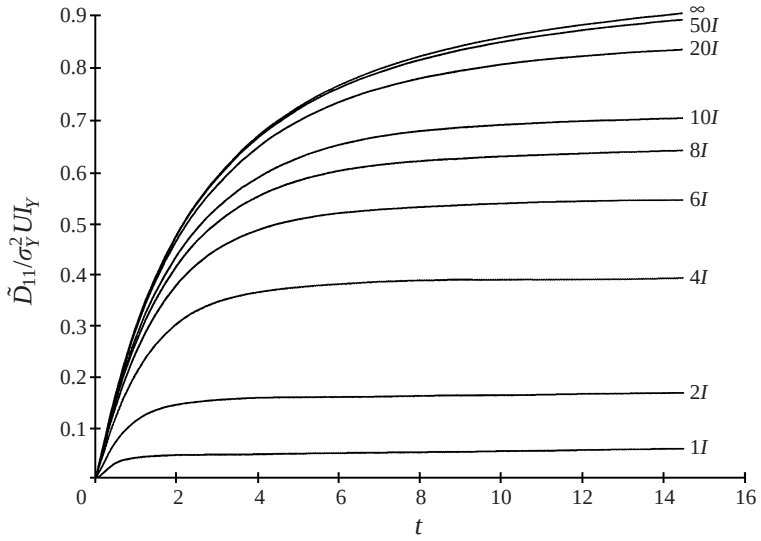

FIGURE 3. The longitudinal block-effective macrodispersion as a function of block scale (marked on each curve) and travel time (equation (42)).

After integration over time and k_2, the following expression, requiring only one integration, is obtained:

$$\widetilde{D}_{11}(t) = D_{11}^{*}(t) - \frac{2\sigma_Y^2 I_1 I_2 U_1}{\pi} \int_0^{\pi/\lambda_1} \sin(U_1 k_1 t) \times \left[\begin{array}{l} \dfrac{a(2a^2 + 3k_1^2 + 2I_1^2 a^2 k_1^2 + I_2^2 a^2 k_1^2 + 3I^2 k_1^4)}{k_1(1 + I_2^2 a^2 + I_1^2 k_1^2)^{1/2}(a^2 + k_1^2)(1 + I_1^2 k_1^2 - I_2^2 k_1^2)^2} \\ \quad - \dfrac{3(1 + I_1^2 k_1^2)}{(1 + I_1^2 k_1^2 - I_2^2 k_1^2)^{5/2}} \tan^{-1}\left(\dfrac{a(1 + I_1^2 k_1^2 - I_2^2 k_1^2)^{1/2}}{k_1(1 + I_2^2 a^2 + I_1^2 k_1^2)^{1/2}} \right) \end{array} \right] \mathrm{d}k_1, \qquad (42)$$

where $a = \pi/\lambda_2$. Figure 3 depicts $\widetilde{D}_{11}$ for various values of $\lambda = \lambda_1 = \lambda_2$. It is observed that larger values of λ lead to larger $\widetilde{D}_{11}$: as the value of λ increases, the portion of the spectrum which is wiped out increases, and hence it must be modelled through macrodispersion coefficients. For λ around $50I_Y$, $\widetilde{D}_{11}$ approaches the macrodispersion coefficient proposed by Dagan (1984). At this range of λ-values, the velocity is modelled only through its expected value, and the effects of the spatial variability in the velocity field on transport are modelled through macrodispersion coefficients. The curves corresponding to smaller λ separate the effects of subgrid-scale variability and supragrid-scale variability. The last effects, represented by the difference between the finite-λ and infinite-λ curves, are the effects of the visible spectrum, captured directly on the numerical grid by construction.

The macrodispersion coefficients are non-local, but they eventually reach a constant, Fickian limit. The rate of approach varies, and increases with λ. This outcome demonstrates the scale dependence of macrodispersion. As the length scale characterizing the wiped-out spectrum becomes smaller, the migrating solute body is sampling the entire range of that spectrum after a shorter travel time, and the Fickian limit is attained earlier.

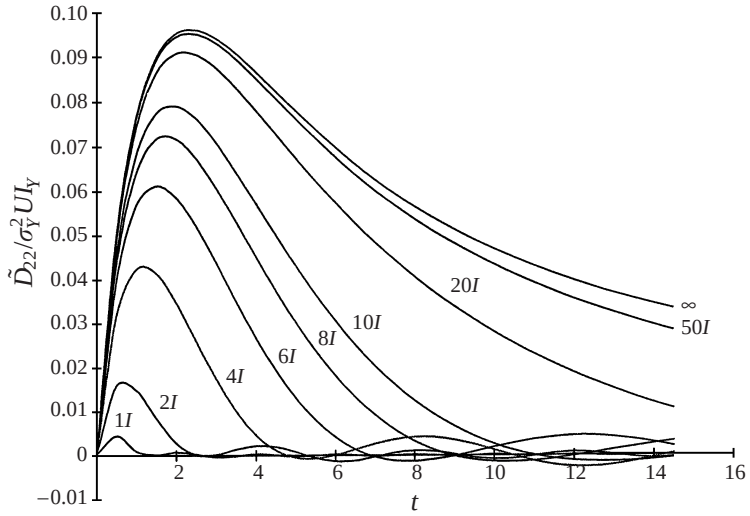

FIGURE 4. The lateral block effective macrodispersion as a function of block scale (marked on each curve) and travel time (equation (43)).

A similar procedure with $i = j = 2$ leads to the following result for the lateral macrodispersion coefficient:

$$\widetilde{D}_{22}(t) = D_{22}^{*}(t) - \frac{\sigma_Y^2 I_1 I_2 U_1}{\pi} \int_0^{\pi/\lambda_1} \sin(U_1 k_1 t) \times \left[\begin{array}{l} -\dfrac{a k_1 (1 + 3I_2^2 a^2 + I_1^2 k_1^2 + 2I_1^2 k_1^2)}{(1 + I_2^2 a^2 + I_1^2 k_1^2)^{1/2} (a^2 + k_1^2)(1 + I_1^2 k_1^2 - I_2^2 k_1^2)^2} \\ + \dfrac{(1 + I_1^2 k_1^2 + 2I_2^2 k_1^2)}{(1 + I_1^2 k_1^2 - I_2^2 k_1^2)^{5/2}} \tan^{-1}\left(\dfrac{a(1 + I_1^2 k_1^2 - I_2^2 k_1^2)^{1/2}}{k_1 (1 + I_2^2 a^2 + I_1^2 k_1^2)^{1/2}} \right) \end{array} \right] \mathrm{d}k_1. \quad (43)$$

$\widetilde{D}_{22}$ is plotted for various λ-values on figure 4. The plot corresponding to $\lambda = \infty$ corresponds to the result published by Dagan (1984), and its asymptotic large-time limit is zero. For λ smaller than ∞, the asymptotic large-time limit is zero as well, but it occurs again at a much earlier time.

6. Numerical examination

Figure 5 compares analytical and numerical results for several values of λ, as a function of time. The results are for $\sigma_Y^2 = 1$. The curve at the top represents the longitudinal macrodispersion coefficient (Dagan 1989), equivalent to the block-effective macrodispersion coefficient in the case $\lambda \to \infty$. Note that this is the coefficient to be used when the velocity field is modelled only through its expected value: in this case, the effects of the spatial variability of the velocity field on mixing are all expressed as dispersive fluxes. For smaller λ, some of that spatial variability is modelled directly over the grid through the advective fluxes, leading to reduction in the macrodispersion coefficient. Hence the difference between the various curves and the curve on the top represents the mixing which is modelled directly through the spatial variability of the velocity field.

The procedure followed for generating these results consists of the following steps: (i) A random Gaussian log-conductivity field is generated. (ii) 'Measurements' are

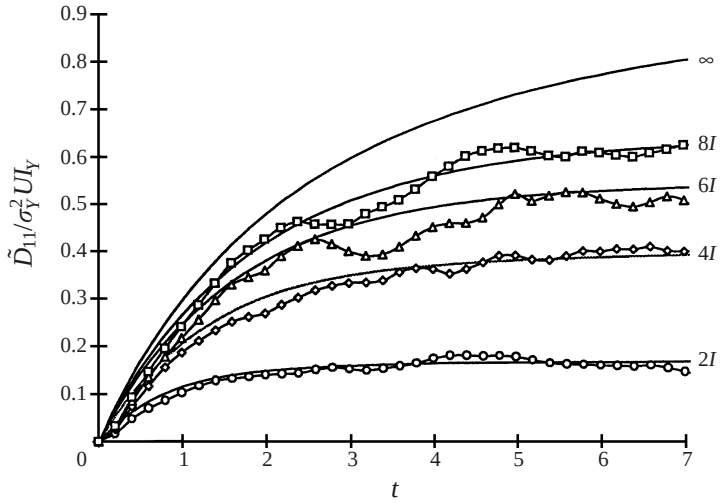

FIGURE 5. A comparison of analytical results for block-effective longitudinal macrodispersion and numerical results. The curve marked ∞ denotes the effective macrodispersion coefficients, which correspond to the case of block size tending to infinity.

then taken at the nodes of the grid with spacing λ. These measurements represent the data available from the field. (iii) To model the effects of the inter-nodal, or unsampled, variability, a series of conditional simulations of the log-conductivity field is conducted, over a grid with spacing much smaller than λ. Note that in conditional simulations, the measurement values at the nodes are fixed and are equal to those taken at step (ii). The log-conductivity fields were generated through HYDRO_GEN (Bellin & Rubin 1996). (iv) The velocity fields corresponding to each log-conductivity field were then determined using a flow field simulator. (v) Transport was simulated through particle tracking: in each realization, the displacement of a single particle was simulated. The number of realizations was determined such that convergence of the ensemble statistics was ensured.

7. A unified approach to the plume scale and grid scale

The issue of plume scale has entered our development so far only through the comparison between the plume's dimension with $I_{\tilde{Y}}$, the integral scale of $\tilde{Y}$. When the plume is much larger, the macrodispersion coefficients developed using the single-particle ensemble statistics model correctly the dispersion process in an experiment. A plume of such dimension is referred to as ergodic.

For modelling transport of non-ergodic plumes, macrodispersion coefficients need to be developed which account for the effects of the plume scale. While very little work has been done so far on the issue of grid scale, there is a large body of work which has been devoted to the issue of plume scale (Kitanidis 1988; Dagan 1991; Rajaram & Gelhar 1993*a*, *b*; Zhang & Lin 1998).

We propose that with a slight change of definitions, the results of the previous sections can be used to address the problem of plume-scale-dependent transport (while ignoring grid-scale issues). Consider a tracer plume of dimensions λ_i, $i = 1, \ldots, m$, moving in a geological environment similar to the one considered in this study. The only portion of the velocity spectrum which contributes to mixing is the high-wavenumber portion, identical to the invisible spectrum in the case of grid block

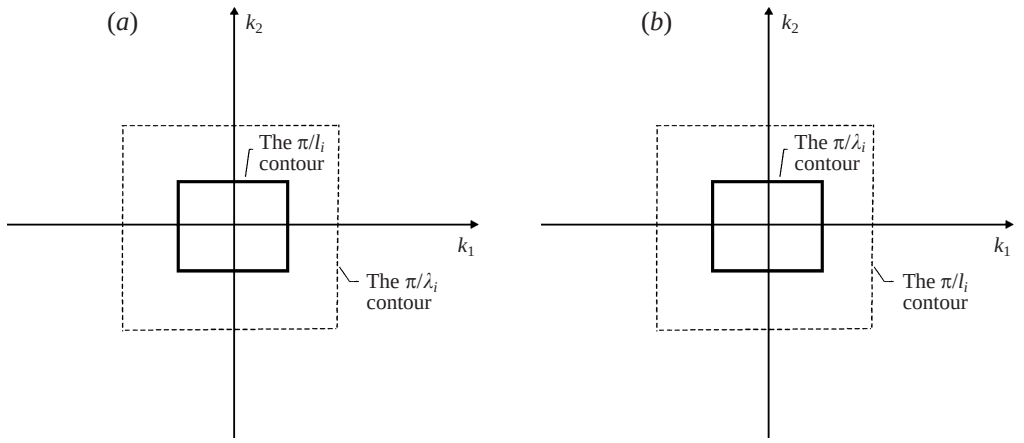

FIGURE 6. (*a*) The effects of the sub-grid variability on dispersion in the case of a large plume. The plume is not affected by wavenumbers inside the solid line. No action is needed to remove these effects. The subgrid variability includes the wavenumbers outside the dashed line. (*b*) The effects of the sub-grid variability on dispersion in the case of a small plume. The plume is affected by wavenumbers outside the dashed line. The block-effective dispersion coefficients need to account only for these wavenumbers. The effects of the wavenumbers in the strip between the solid line and dashed line should be eliminated. That strip will keep decreasing in size as the plume increases in dimension.

scales λ_i which we considered in previous sections. For this problem definition, a solution was presented by Rajaram & Gelhar (1993*b*, equation 37*a*, with $1-\overline{F}$ there equal to our F) which is identical to our (37). The surprising conclusion is that the block-scale and plume-scale transport problems have a common solution.

We wish now to combine the effects of both grid scale and plume scale. The grid scales are, as previously, λ_i. Additionally, we denote the plume scales at time t by $l_i(t)$. Recalling that the grid's Nyquist numbers π/λ_i define lower cut-offs on the variability captured by the grid (wiped-out variability is $k_i > \pi/\lambda_i$) while the plume's Nyquist numbers $\pi/l_i(t)$ define lower cut-offs on the variability affecting the plume's dispersion, the following two situations need to be considered (figure 6):

(i) The case of $\pi/\lambda_i > \pi/l_i(t)$, see figure 6(*a*). This is the case of a plume larger than the grid block. The plume's Nyquist numbers will filter the effects of the $k_i > \pi/l_i(t)$ which are simulated directly on the grid. The smaller-scale variability is either simulated on the grid or modelled through the block-effective dispersion tensor. Hence the plume's scale does not affect the block-effective macrodispersivities.

(ii) The case of $\pi/\lambda_i < \pi/l_i(t)$, see figure 6(*b*). This is the case of a plume smaller than the grid block. This case is problematic since the plume is dispersed over the block regardless of the dispersion coefficient. But $\widetilde{D}_{ij}$ in this case can be used to compute when the plume reaches the block size, and case (i) applies. Here there is a range of subgrid-scale variability which does not affect the plume's dispersion, and the block-effective dispersivities need to be modified. This can be achieved by modifying (37) to the following form:

$$\widetilde{D}_{ij}(t) = D^*_{ij}(t) - \frac{1}{(2\pi)^{m/2}} \int_0^t \left[\int_{-\pi/\Omega_1}^{\pi/\Omega_1} \cdots \int_{-\pi/\Omega_m}^{\pi/\Omega_m} \mathrm{e}^{-\mathrm{i}\boldsymbol{k}\cdot\boldsymbol{U}t'} U_q U_p \right.$$

$$\left. \times \left\{ \delta_{jq} - \frac{k_j k_q}{k^2} \right\} \left\{ \delta_{lp} - \frac{k_l k_p}{k^2} \right\} C_Y(\boldsymbol{k})\, \mathrm{d}\boldsymbol{k} \right] \mathrm{d}t' \tag{44}$$

with

$$\Omega_i = \begin{cases} l_i(t) & \text{for } l_i(t) < \lambda_i \\ \lambda_i & \text{otherwise.} \end{cases} \tag{45}$$

The significance of (44) is that it accounts for the effects of both the grid block scale and plume scale. This unified approach is important in applications and is reported here, to our knowledge, for the first time.

For $l_i \sim 0$ the second term on the right-hand side of (44) equals $D^*_{ij}(t)$, and hence $\widetilde{D}_{ij}(t) = 0$, and the solute body does not disperse at all. The case of $l_i > \lambda_i$ is addressed by the second condition in (45) and is the one addressed in previous sections. But it is recalled that the ergodic limit occurs only for $l_i \gg I_{\tilde{Y}}$. Following Dagan (1991), this inequality should hold in at least one direction orthogonal to the mean flow direction. Under non-ergodic conditions, the block-effective macrodispersion coefficients represent average behaviour, and not a single experiment.

8. On the effects of pore-scale dispersion

Variability at the scale of the pore leads to pore-scale dispersion. The significance of pore-scale dispersion depends on the process which is modelled, and the ratio between I_Y and a characteristic length scale of the pore, known as the Péclet number. At large Péclet numbers, the pore-scale dispersion's contribution to the evolution of the spatial moments of a solute body can be simply added to the contribution of the variability of the conductivity (Fiori 1996). At smaller Péclet numbers there is an increase in the interaction between the pore-scale and large-scale effects. Consider for example transport in a domain composed of thin layers of different permeabilities with flow in the direction of the layers. It is easy to visualize that pore-scale dispersion transfers mass across layers which in turn enhances the longitudinal dispersion. The formalism developed in the previous sections allows the effects of pore-scale variability on the block-effective dispersivity to be introduced.

To address this issue we adopt Corrsin's conjecture (Lundgren & Pointin 1975) and modify it for consistency. Corrsin's conjecture has been pursued by Dagan (1987, 1989) and Neuman & Zhang (1990) in their work on macrodispersion. Employing Corrsin's conjecture and adopting the equality (30), the Lagrangian velocity covariance is obtained as follows:

$$v_{ij}(t) = \frac{1}{(2\pi)^{m/2}} \int_{-\infty}^{\infty} \dots \int_{-\infty}^{\infty} \exp\left(\mathrm{i}\boldsymbol{k}\cdot\boldsymbol{U}t - \boldsymbol{k}\cdot\boldsymbol{D}_d\cdot\boldsymbol{k}^T t\right) \times \langle \exp(\mathrm{i}\boldsymbol{k}\cdot\boldsymbol{X}')\rangle U_q U_p \left\{\delta_{jq} - \frac{k_j k_q}{k^2}\right\}\left\{\delta_{lp} - \frac{k_l k_p}{k^2}\right\} C_Y(\boldsymbol{k})\,\mathrm{d}\boldsymbol{k} \tag{46}$$

where $\boldsymbol{D}_d$ is the pore-scale dispersion tensor, $\boldsymbol{X}'$ is defined in (26), and the superscript T denotes transpose. Note that the exponential in angled brackets introduce terms of order higher than σ_Y^2 and can be approximated by unity for consistency (Dagan 1987; Fiori 1996). Introducing the filter F (see equation (37)) and integrating (46) over time, leaves

$$\widetilde{D}_{ij}(t) = \frac{1}{(2\pi)^{m/2}} \int_{-\infty}^{\infty} \dots \int_{-\infty}^{\infty} \frac{\exp\left(\mathrm{i}\boldsymbol{k}\cdot\boldsymbol{U}t - \boldsymbol{k}\cdot\boldsymbol{D}_d\cdot\boldsymbol{k}^T t\right) - 1}{\mathrm{i}\boldsymbol{k}\cdot\boldsymbol{U} - \boldsymbol{k}\cdot\boldsymbol{D}_d\cdot\boldsymbol{k}^T} \times U_q U_p \left\{\delta_{jq} - \frac{k_j k_q}{k^2}\right\}\left\{\delta_{lp} - \frac{k_l k_p}{k^2}\right\} F(\boldsymbol{k})\, C_Y(\boldsymbol{k})\,\mathrm{d}\boldsymbol{k}. \tag{47}$$

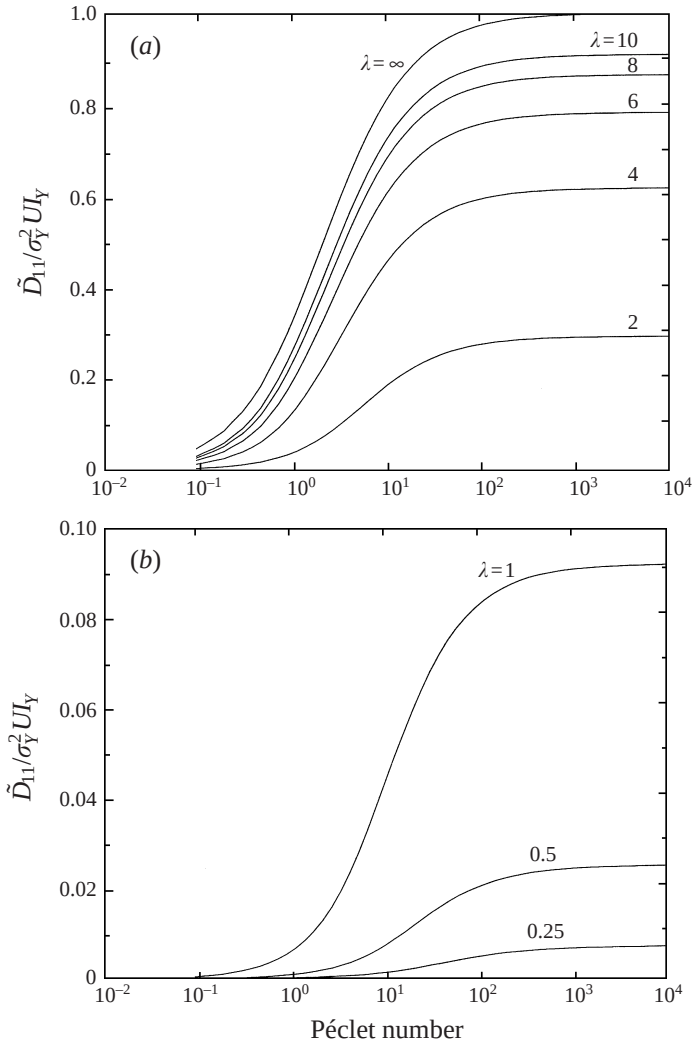

FIGURE 7. The large-time asymptotic limits of the longitudinal block-effective dispersivity $\widetilde{D}_{11}$ as a function of the grid spacing λ and the Péclet number (UI_Y/D_d). The results are obtained based on equation (47).

The large-time asymptotic limits of $\widetilde{D}_{11}$ based on the method of Fiori (1996) are plotted on figure 7 as functions of the Péclet number (defined as UI_Y/D_d) for various block dimensions. The tensor $\boldsymbol{D}_d$ was assumed here to be diagonal and isotropic, with the elements along the diagonal equal to D_d. We find $\widetilde{D}_{11}$ to be insensitive to pore-scale dispersion at the range of Péclet numbers usually encountered in field applications (>100). At smaller Péclet numbers pore-scale dispersion acts to reduce $\widetilde{D}_{11}$, and its effects are more pronounced for smaller grid size λ. As λ decreases, the wiped-out variability is composed of larger $\boldsymbol{k}$, and the dumping effect of $\boldsymbol{D}_d$ in (46) is enhanced.

9. Discussion

A tensor $\widetilde{D}_{ij}$ is developed for introducing the effects of subgrid variability on mixing of tracers in porous media. Based on a SRF model for the spatial variability of the

log-conductivity, this tensor models the dispersive flux resulting from the spatial variability that becomes 'invisible' in numerical models when the grid block scale is large compared to the integral scale of the log-conductivity. Previous works (Ababou *et al.* 1989) have shown that the need for such tensor arises when the grid-block scale exceeds about a quarter of the log-conductivity integral scale.

The theory presented here extends and combines the Lagrangian theory of Dagan (1984) with the spectral conditioning approach presented by Ababou & Gelhar (1990). The basic idea is to separate the variability of the conductivity that is visible through measurements taken with spacing of characteristic length λ, and that which is invisible and hence unaccounted for. The block-effective macrodispersion tensor is intended to capture the effects of the variability which becomes invisible due to partial sampling.

The length scale λ need not be the typical spacing of measurements in the field. It can also represent the numerical grid-block scale with measurements specified at the nodes or centres of the grid blocks, as commonly done in Monte Carlo simulations. A major benefit of the proposed theory is in allowing conditioning the flow and transport simulation on field data. This is achieved by incorporating the field data in the flow model, and recognizing only the unmodelled heterogeneity in the transport part. For modelling, such an approach is appealing.

Another length scale of significance is the scale of the solute plume l, which introduces another filter (Dagan 1991; Rajaram & Gelhar 1993*a*, *b*, 1995). The limited plume dimension acts to suppress the effects of the low-wavenumber fluctuations, and hence it needs to be recognized only when it is smaller than λ. Our theory addressed this aspect, and the block-effective dispersion tensor can be modified to account for the suppressed variability due to grid-block scale and plume scale. We showed that the plume scale needs to be accounted for directly, i.e. through the dispersion tensor, only when the plume's scale is smaller than the grid-block's scale. When the plume is larger, the variability which is affecting it is modelled in part through the block-effective macrodispersion tensor or directly over the grid.

Reliable modelling of transport in the subsurface requires that models be conditioned on measurements of variables such as conductivity, pressure and velocity (Rubin 1991*a,b*, 1997; Rubin & Dagan 1992). Macrodispersion theories ignored this aspect. The justification is that the effects of data are only local and need not be considered when modelling transport of large solute bodies. Such solute bodies have been referred to as ergodic (Dagan 1991), and their displacement and dispersion are controlled by effective parameters and not local values. This is no longer true when dealing with non-ergodic solute bodies. Our approach addresses this issue systematically. We propose that a numerical grid can be developed with the grid block at the scale of the spacing between measurements. This grid captures the low-wavenumber portion of the variability. The block-effective dispersion tensor captures the high-wavenumber portion. That tensor is in general non-stationary, and it depends on local values of the conductivity. For domains of small variance in the log-conductivity these effects are minor and negligible.

To our knowledge, no theory exists which accounts for grid-scale, plume-scale, and pore-scale dispersion collectively, while allowing transport models to be conditioned on field measurements. A brief perspective on previous works on block-effective dispersion coefficients is now given. Works in these area addressed separately the issues of block scale and grid scale. Plume-scale issues were addressed in Kitanidis (1988), Dagan (1991), Rajaram & Gelhar (1993*a*, *b*) and more recently Zhang & Lin (1998). Much less work has been done on issues of grid scale. The two studies reported below addressed the issue through either conjectures or idealized mathematical constructs, but no general framework has been provided.

To address the grid-scale issue, Dagan (1994) modelled the solute plume as being composed of a series of sub-plumes, each of the size of the grid block. He then assumed that the suppression of the subgrid-scale variability entails that each subplume moves in the aquifer isomorphically, and developed the block-effective coefficients to compensate for the discrepancy. In this approach the large-scale–small-scale variability interactions are neglected. The results of Dagan (1994) are close to, though somewhat higher than, the results of the present study. That work did not address plume-scale issues and pore-scale dispersion. Liu & Molz (1997) made a conjecture regarding the large-time, asymptotic limit of the longitudinal block-effective macrodispersion coefficient which is in agreement with the asymptotic limit presented here but under the conditions of small variability in the log-conductivity. That work did not address plume-scale issues, pore-scale dispersion issues, the pre-asymptotic behaviour or the lateral dispersion terms.

The help of Dr Fiori in producing figure 7 is appreciated. We acknowledge with gratitude the comments and suggestions made by our reviewers. This study was supported by NSF Hydrologic Sciences Program through grant EAR-9628306, and by DOE's ESMP program through grant DE-FG07-96ER14726.

Appendix

The Fourier transform (FT) pair is defined here through an example using C_Y, the spatial covariance of Y. The FT is

$$C_Y(\boldsymbol{k}) = \frac{1}{(2\pi)^{m/2}} \int_{-\infty}^{\infty} \dots \int_{-\infty}^{\infty} C_Y(\boldsymbol{r}) \exp(\mathrm{i}\boldsymbol{k}\cdot\boldsymbol{r})\, \mathrm{d}\boldsymbol{r}, \tag{A 1}$$

where $\mathrm{d}\boldsymbol{r} = \mathrm{d}r_1 \dots \mathrm{d}r_m$. The inverse transform is defined as follows:

$$C_Y(\boldsymbol{r}) = \frac{1}{(2\pi)^{m/2}} \int_{-\infty}^{\infty} \dots \int_{-\infty}^{\infty} C_Y(\boldsymbol{k}) \exp(-\mathrm{i}\boldsymbol{k}\cdot\boldsymbol{r})\, \mathrm{d}\boldsymbol{k}. \tag{A 2}$$

The FT pair defined here is slightly different from the conventional one in terms of the coefficient preceding the integrals. Its benefit to us is its symmetry, with the exception of the sign of i. We shall refer to $C_Y(\boldsymbol{k})$ and other FTs of covariances as *radial spectra*. The radial spectrum can be converted to the customary spectrum using

$$S_Y(\boldsymbol{k}) = \frac{1}{(2\pi)^{m/2}} C_Y(\boldsymbol{k}). \tag{A 3}$$

We recall some basic properties of the radial spectrum of the velocity in Fourier space and their relationship with their counterparts in physical space. The radial spectrum of the velocity covariance is the Fourier transform of the velocity covariance in physical space:

$$\tilde{u}_{ij}(\boldsymbol{k}) = \mathrm{FT}[\tilde{u}_{ij}(\boldsymbol{r})], \tag{A 4}$$

where $\boldsymbol{r}$ is the separation distance vector. Defining further $\tilde{u}_j(\boldsymbol{k}) = \mathrm{FT}[\tilde{u}_j(\boldsymbol{x})]$, it can be shown that

$$\langle \tilde{u}_i(\boldsymbol{k}) \tilde{u}_j^*(\boldsymbol{k}') \rangle = (2\pi)^{m/2} \tilde{u}_{ij}(\boldsymbol{k}) \delta(\boldsymbol{k} - \boldsymbol{k}'), \tag{A 5}$$

where the asterisk denotes the complex conjugate. Similarly, from (22), for $\tilde{u}_i(\boldsymbol{k}) = a_i \widetilde{Y}(\boldsymbol{k})$ and $\tilde{u}_j^*(\boldsymbol{k}) = a_j \widetilde{Y}^*(\boldsymbol{k})$, we have

$$\langle \tilde{u}_i(\boldsymbol{k}) \tilde{u}_j^*(\boldsymbol{k}') \rangle = (2\pi)^{m/2} a_i a_j C_{\widetilde{Y}}(\boldsymbol{k}) \delta(\boldsymbol{k} - \boldsymbol{k}'), \tag{A 6}$$

which, when matched with (A 5), leads to (23). For additional discussion see Dagan (1989).

REFERENCES

Ababou, R. & Gelhar, L. W. 1990 Self-similar randomness and spectruml conditioning: Analysis of scale effects in subsurface hydrology. In *Dynamics of Fluids in Hierarchical Porous Media* (ed. J. Cushman). Academic.

Ababou, R., McLaughlin, D., Gelhar, L. & Tompson, A. F. B. 1989 Numerical simulation of three-dimensional saturated flow in randomly heterogeneous porous media. *Transport Porous Media* **4**, 549–565.

Beckie, R., Aldama, A. A. & Wood, E. F. 1996 Modeling the large scale dynamics of saturated groundwater flow using spatial filtering theory, 1. Theoretical development. *Water Resour. Res.* **32**, 1269–1280.

Bellin, A. & Rubin, Y. 1996 HYDRO_GEN: A spatially distributed random field generator for correlated properties. *Stoch. Hydrol. Hydraul.* **10**(4), 253–278.

Bellin, A., Salandin, P. & Rinaldo, A. 1992 Simulation of dispersion in heterogeneous porous formations: Statistics, first-order theories, convergence of computations. *Water Resour. Res.* **28**, 2211–2227.

Bras, R. L. & Rodriguez-Iturbe, I. 1985 Random Functions in Hydrology. Addison Wesley.

Chin, D. A. 1997 An assessment of first-order stochastic dispersion theories in porous media. *J. Hydrol.* **199**, 53–73.

Cushman, J. H., Deng, F.-W. & Hu, X. 1995 A non local theory of reactive transport with physical and chemical heterogeneity: localization errors. *Water Resour. Res.* **31**, 2239–2255.

Dagan, G. 1984 Solute transport in heterogeneous porous formations. *J. Fluid Mech.* **145**, 151–177.

Dagan, G. 1985 Stochastic modeling of groundwater flow by unconditional and conditional probabilities: The inverse problem. *Water Resour. Res.* **21**, 65–72.

Dagan, G. 1987 Theory of solute transport by groundwater. *Ann. Rev. Fluid Mech.* **19**, 183–215.

Dagan, G. 1989 Flow and Transport in Porous Formations. Springer.

Dagan, G. 1991 Dispersion of a passive solute in non-ergodic transport by steady velocity fields in heterogeneous formations. *J. Fluid Mech.* **233**, 197–210.

Dagan, G. 1994 Upscaling of dispersion coefficients in transport through heterogeneous formations. In *Computational Methods in Water Resources X*, pp. 431–439. Kluwer.

Dykkar, B. B. & Kitanidis, P. K. 1992 Determination of the effective hydraulic conductivity of heterogeneous porous media, using a numerical spectruml approach. *Water Resour. Res.* **28**, 1167–1178.

Fiori, A. 1996 Finite Péclet extensions of Dagan's solutions to transport in anisotropic heterogeneous formations. *Water Resour. Res.* **32**, 193–198.

Gelhar, L. 1993 *Stochastic Subsurface Hydrology*. Prentice Hall.

Gelhar, L. W. & Axness, C. L. 1983 Three-dimensional stochastic analysis of macrodispersion in aquifers. *Water Resour. Res.* **19**, 161–180.

Hu, B. X., Deng, F.-W. & Cushman, J. H. 1997 Non-local reactive transport with physical and chemical heterogeneity: linear nonequilibrium sorption with random rate coefficients. In *Subsurface Flow and Transport: A Stochastic Approach* (ed. G. Dagan & S. P. Neuman). Cambridge University Press.

Kitanidis, P. K. 1988 Prediction by the methods of moments of transport in a heterogeneous formation. *J. Hydrology* **102**, 453–473.

Liu, H. H. & Molz, F. J. 1997 Block scale dispersivity for heterogeneous porous media characterized by stochastic fractals. *Geophys Res. Lett.* **24**, 2239–2242.

Lundgren, T. S. & Pointin, Y. B. 1975 Turbulent self-diffusion. *Phys. Fluids* **19**, 355–361.

Neuman, S. P. & Orr, S. 1993 Prediction of steady state flow in non-uniform geologic media by conditional moments; exact nonlocal formalism, effective conductivities and weak approximation. *Water Resour. Res.* **29**, 633–645.

Neuman, S. P. & Zhang, Y. K. 1990 A quasi-linear theory of non-Fickian and Fickian subsurface dispersion, 1, Theoretical analysis with application to isotropic media. *Water Resour. Res.* **26**, 887–902.

RAJARAM, H. & GELHAR, L. W. 1993*a* Plume-scale dependent dispersion in heterogeneous aquifers, 1, Lagrangian analysis in a stratified aquifer. *Water Resour. Res.* **29**, 3249–3260.

RAJARAM, H. & GELHAR, L. W. 1993*b* Plume-scale dependent dispersion in heterogeneous aquifers, 2, Eulerian analysis and three-dimensional aquifers. *Water Resour. Res.* **29**, 3261–3276.

RAJARAM, H. & GELHAR, L. 1995 Plume scale dependent dispersion in aquifers with a wide range of scales of heterogeneity. *Water Resour. Res.* **31**, 2469–2482.

RUBIN, Y. 1990 Stochastic modeling of macrodispersion in heterogeneous porous media. *Water Resour. Res.* **26**, 133–142.

RUBIN, Y. 1991*a* Prediction of tracer plume migration in disordered porous media by the method of conditional probabilities. *Water Resour. Res.* **27**, 1291–1308.

RUBIN, Y. 1991*b* Transport in heterogeneous porous media; prediction and uncertainty. *Water Resour. Res.* **27**, 1723–1738.

RUBIN, Y. 1997 Transport of inert solutes by groundwater: recent development and current issues. In *Subsurface Flow and Transport: A Stochastic Approach* (ed. G. Dagan & S. P. Neuman). Cambridge University Press.

RUBIN, Y. & DAGAN, G. 1992 Conditional estimation of solute travel time in heterogeneous formations, 1, Impact of transmissivity measurements. *Water Resour. Res.* **28**, 1033–1044.

RUBIN, Y., HUBBARD, S. S., WILSON, A. & CUSHEY, M. A. 1998 Aquifer characterization. In *The Handbook of Groundwater Engineering* (ed. J. W. Delleur). CRC Press.

ZHANG, Y. K. & LIN, J. 1998 Numerical simulation of transport of non-ergodic solute plumes in heterogeneous aquifers. *Stoch. Hydrol. Hydraul.* **12**, 117–139.